Synthesis of Pure Metastable Wurtzite CZTS Nanocrystals by Facile One-Pot Method

ARTICLE *in* THE JOURNAL OF PHYSICAL CHEMISTRY C · DECEMBER 2012

Impact Factor: 4.77 · DOI: 10.1021/jp307346k

THE JOURNAL OF PHYSICAL CHEMISTRY C

Article

pubs.acs.org/JPCC

Synthesis of Pure Metastable Wurtzite CZTS Nanocrystals by Facile One-Pot Method

Mei Li, Wen-Hui Zhou,* Jie Guo, Yan-Li Zhou, Ze-Liang Hou, Jie Jiao, Zheng-Ji Zhou, Zu-Liang Du, and Si-Xin Wu*

The Key Laboratory for Special Functional Materials of MOE, Henan University, Kaifeng 475004, China

Supporting Information

ABSTRACT: In this article, pure phase metastable wurtzite Cu_2ZnSnS_4 (CZTS) nanocrystals (NCs) were synthesized by a facile one-pot method. When pure 1-dodecanethiol (DDT) was used as the solvent, two coexisting CZTS phases (wurtzite and kesterite) were found. When an increased amount of oleylamine (OAm) was added to DDT, kesterite CZTS disappeared gradually, and the as-obtained CZTS NCs became smaller and more uniform. When 0.5 mL of OAm was added, rice-like pure phase metastable wurtzite CZTS NCs were obtained. The factors, including amount of OAm, reaction temperature, reaction time, and concentration of precursors, which influence the morphology, size, and monodispersity of CZTS NCs, were studied in detail. The results showed OAm played an important role in the formation of the final pure phase metastable wurtzite NCs. Time-dependent experiments were performed to observe the growth of CZTS NCs. The final CZTS NCs evolved from spherical-like Cu_2S NCs through rhombus-like intermediate shaped NCs to rice-like pure wurtzite CZTS NCs. On the basis of the detailed time-dependent shape and elemental composition evolutions, a possible asynchronous doping growth and formation mechanism was proposed. The optical and electrical properties of the pure wurtzite CZTS NCs were also investigated. The band gap of the rice-like CZTS is about 1.49 eV, which approaches the optimum value for solar photoelectric conversion. Meanwhile, the current−voltage characteristics and Hall effect measurement of the wurtzite CZTS NCs films indicated that rice-like CZTS NCs favored the electronic transmission and thus may induce the generation of photocurrent. Thus, the obtained wurtzite CZTS NCs are more suitable for using as absorber layer in low cost solar cells.

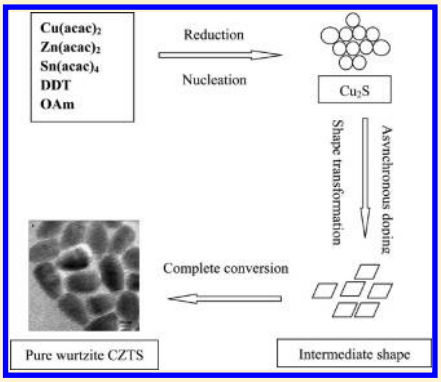

1. INTRODUCTION

CZTS, a direct band gap semiconductor, is a quaternary chalcogenide semiconductor with high absorption coefficient in the visible region (over 10^4 cm^{-1}). The band gap of CZTS is about 1.4−1.6 eV, which is very close to the optimum value for being used as an absorber layer in solar cells.[1−3] Compared to $CuIn_xGa_{1-x}(Se)_2$ (CIGS) or $CuInS_2$ (CIS), CZTS is nontoxic, and the elements are abundant in the crust of the earth (the crustal abundance of Zn and Sn is 1500 times and 45 times greater than that of In, respectively). While the price of Zn and Sn is almost 2 orders of magnitude lower than that of In.[4] Owing to these special properties, CZTS has attracted considerable attention in the field of low cost, environmentally friendly thin film solar cells.[1,3] Nakayama et al. first successfully prepared stannite CZTS thin film by the spray pyrolysis.[5] The first fabricated CZTS-based solar cells with Al/ZnO/CdS/CZTS/Mo/SLG architecture provided an efficiency of 0.66%.[6] To date, the highest performing champion of CZTS-based solar cells (independent of deposition approach) show efficiencies of 8.4%[7] and 10.1%[8] for pure sulfur (CZTS) and mixed selenosulfur (CZTSSe) system, respectively.[9]

Because nanocrystals (NCs) inks can be sprayed, spin-, or dip-coated onto substrates directly and easily, solution-based method to synthesize CZTS NCs have attracted extensive attention. Recently, CZTS NCs had been prepared by several groups using the hot-injection method.[10−14] The traditionally obtained CZTS NCs are always in the kesterite or stannite phase, which features a tetragonal crystal cell.[11,15−19] Recently, several groups have reported the synthesis of wurtzite phase CZTS NCs by hot-injection,[19,20] noninjection,[21] and hydrothermal method.[22] However, the hot-injection and noninjection synthetic procedure still require relatively complex and costly operation, such as inert gas protection (nitrogen or argon), stepwise heating, and relatively high reaction temperature (≥240 °C), and the major shortcoming of hydrothermal method is the lack of good control over particle size, morphology, and monodispersity of the products. Therefore, a facile and inexpensive method for the preparation of high quality, monodisperse, and pure phase wurtzite CZTS NCs is still highly demanded.

Herein, we describe a low-cost and convenient one-pot method for the preparation of pure phase metastable wurtzite CZTS NCs under atmospheric conditions. The proposed method was carried out at relatively low temperature and did

Received: July 25, 2012
Revised: November 9, 2012
Published: November 29, 2012

   dx.doi.org/10.1021/jp307346k | J. Phys. Chem. C 2012, 116, 26507−26516

not require noble gas. Compared to other synthetic procedures for wurtzite CZTS NCs, we adopted the simple one-pot method using one-step heating to synthesize wurtzite CZTS NCs at low temperature, which is relatively simple and economical. During the formation of pure phase metastable wurtzite CZTS NCs, OAm plays an important role in the process of the CZTS phase transition from tetragonal and hexagonal structures. Transmission electron microscopy (TEM), energy dispersive spectrometry (EDS), X-ray diffraction (XRD), and X-ray photoelectron spectroscopy (XPS) characterizations confirm the structure, composition, morphology, and valence state of as-obtained wurtzite CZTS NCs. Optical and electrical characterizations indicated that wurtzite CZTS NCs may favor the electronic transmission and thus induce the generation of photocurrent. Thus, the obtained wurtzite CZTS NCs are more suitable for solar energy conversion applications and may have great potential to be applied in high-efficiency, yet low-cost solar cells areas.

2. EXPERIMENTAL SECTION

2.1. Materials. Copper(II) chloride dihydrate ($CuCl_2$), zinc(II) chloride ($ZnCl_2$), tin(IV) chloride tetrahydrate ($SnCl_4$), 2,4-pentanedione, and triethylamine were the products of Alfa. Oleylamine (OAm) and 1-dodecanethiol (DDT) were obtained from Sigma. Other chemicals were all of analytical grade and used without any further purification. All water used was obtained from a Millipore Milli-Q purification system.

2.2. Preparation of the Wurtzite CZTS NCs. *2.2.1. Synthesis of the Cu(acac)$_2$, Zn(acac)$_2$, and Sn(acac)$_4$.* For the synthesis of $Sn(acac)_4$, 20 mmol of $SnCl_4$ was dissolved in 15 mL of deionized water. Under magnetic stirring, 90 mmol of 2,4-pentanedione (9 mL) was added and kept stirring for another 15 min. Then, $Sn(acac)_4$ was precipitated by the addition of triethylamine (~6 mL). The resulting $Sn(acac)_4$ was washed for several times by ethanol and water, then dried in the vacuum for further use. The synthesis of $Cu(acac)_2$ and $Zn(acac)_2$ were similar to that of $Sn(acac)_4$.

2.2.2. Synthesis of the Wurtzite CZTS NCs by One-Pot Route. In a typical experimental procedure, 10 mL of DDT, 0.5 mL of OAm, 0.1 mmol of $Sn(acac)_4$ (53 mg), 0.1 mmol of $Zn(acac)_2$ (28 mg), and 0.2 mmol of $Cu(acac)_2$ (56 mg) were mixed in a 50 mL flask with the aid of magnetic stirring. Then, the mixture was heated to 220 °C in an oil bath and held for 4 h. After being cooled to room temperature, the CZTS NCs were separated by precipitation with the addition of ethanol and then collected by centrifugation at 9500 rpm for 4 min. The supernatant was decanted, while the precipitates were dispersed in the hexane and further purified by ethanol several times. Final products were obtained and dried in a vacuum oven overnight at room temperature for further characterizations. The synthesis of different CZTS NCs was performed by changing one of the experimental parameters as indicated. In order to ascertain the growth and formation mechanism (shape evolution) of CZTS NCs, time-dependent experiments were performed, and aliquots were taken out with a syringe at different times (30 min, 40 min, 50 min, 1 h, 2 h, 4 h, 8 h, and 24 h) to monitor the growth of CZTS NCs during the reaction.

2.3. Characterization. The morphology of CZTS NCs was characterized by field emission scanning electron microscopy (FESEM, JEOL JSM-7001F) and transmission electron microscopy (TEM, JSM-2010). High-resolution transmission electron microscopy (HRTEM) observation was performed using a JEOL JEM-2010 microscope with an accelerating voltage of 200 kV. The phase and crystallographic structure of the products were identified by X-ray diffraction (XRD, Philips X' Pert Pro, Cu−Kα; λ = 0.154056 nm). The chemical composition of products was analyzed by energy dispersive spectrometry (EDS, Horiba EMAX Energy EX-350). The UV−vis absorption spectra were obtained by using a UV−vis spectrometer (Perkin-Elmer, Lambda 35). An $I-V$ curve was measured by the Semiconductor Characteristic Measurement System (Model SCS/F'-4200). The carrier concentration, Hall mobility, and electrical resistivity were obtained by the four-probe van der Pauw method using Hall-effect measurement system (HMS-3000, ECOPIA) in a magnetic field strength of 0.51 T at room temperature. X-ray photoelectron spectroscopy (XPS) measurements were carried out on an AXIS ULTRA spectrometer using Al Kα X-ray as the excitation source. The Raman spectrum was recorded using a LABRAM-1B confocal laser micro-Raman spectrometer with the wavelength of 632.8 nm.

3. RESULTS AND DISCUSSION

3.1. Synthesis of Pure Phase Metastable Wurtzite CZTS NCs. A series of CZTS NCs were synthesized using DDT as the solvent and sulfur source at 220 °C. The XRD patterns of CZTS NCs synthesized with different amounts of OAm are shown in Figure 1. The major diffraction peaks of as-

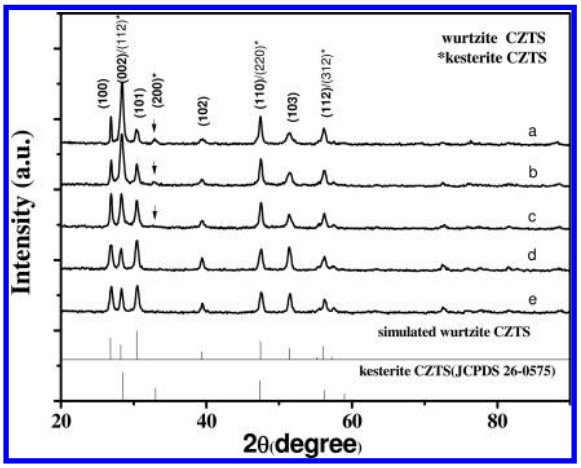

Figure 1. XRD patterns of CZTS NCs obtained in (a) pure DDT, (b) DDT + 0.1 mL of OAm, (c) DDT + 0.2 mL of OAm, (d) DDT + 0.5 of mL OAm, and (e) DDT + 1 mL of OAm.

synthesized CZTS NCs can be indexed to kesterite CZTS (JCPDS 26-0575) and/or cation-disordered wurtzite CZTS proposed by Peng et al.[19] Because the arrangements of atoms in two crystal structures (kesterite and simulated wurtzite) are basically similar, the three strongest diffraction peaks (appeared at about 28°, 47°, and 56°) of these two structures are almost at the same positions.[22] In other words, the diffraction peaks that appeared at about 28°, 47°, and 56° can be attributed to (112), (220), and (312) planes of kesterite CZTS or (002), (110), and (112) planes of wurtzite CZTS, respectively. The diffraction peaks that appeared at about 27°, 30°, 39°, and 51° are attributed to (100), (101), (102), and (103) planes of wurtzite CZTS. The weak diffraction peak at around 33°, which correspond to the (200) plane of kesterite CZTS, could be used to track the phase formation during the formation of CZTS NCs. When pure DDT was used as the solvent, two coexisting CZTS phases (wurtzite and kesterite) were found

dx.doi.org/10.1021/jp307346k | J. Phys. Chem. C 2012, 116, 26507−26516

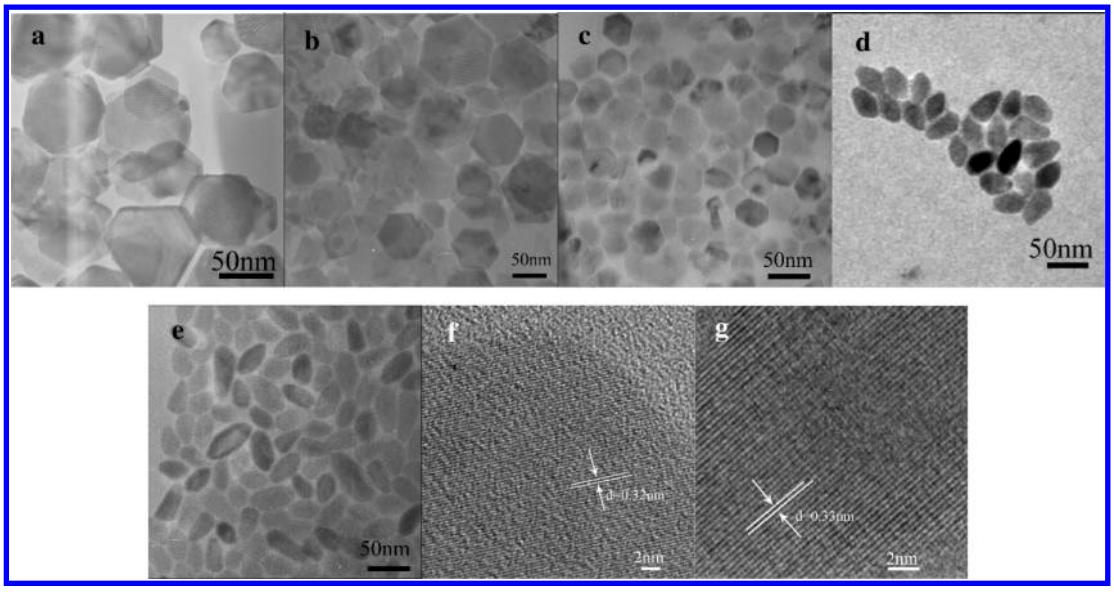

Figure 2. TEM images of CZTS NCs obtained in (a) pure DDT, (b) DDT + 0.1 mL of OAm, (c) DDT + 0.2 mL of OAm, (d) DDT + 0.5 mL of OAm, and (e) DDT + 1 mL of OAm; HRTEM images of CZTS NCs obtained in (f) pure DDT and (g) DDT + 0.5 mL of OAm.

(Figure 1a). When an increased amount of OAm was added to DDT, the diffraction peak of the kesterite CZTS (200) plane became weaker and weaker until it completely disappeared, while the diffraction peak of the wurtzite CZTS (002) plane was also suppressed gradually. These results indicated that the kesterite CZTS in as-synthesized CZTS NCs disappeared gradually (Figure 1a–d). In other words, the diffraction pattern gradually evolves from that of coexisting phases to pure wurtzite as the amount of OAm increases. When 0.5 mL or more than 0.5 mL (1 mL) of OAm was added, pure phase metastable wurtzite CZTS NCs were obtained (Figure 1d,e). The lattice parameters ($a = b = 3.83$ Å; $c = 6.31$ Å) of the typical sample (0.5 mL OAm) refined by the Jade 5 software are similar to the reported data by Peng (space group, *P*63*mc*, and unit cell dimensions, $a = b = 3.8387$ Å and $c = 6.3388$ Å).[19] The difference maybe caused by the peak shift during the measurement process. It had been reported that DDT is the key factor for the formation of wurtzite CZTS rather than kesterite CZTS.[19] DDT could react with different metal cations to produce different metal thiolates, which would decompose into corresponding sulfides at certain temperature.[23−25] In our study, we adopted a one-pot method using one-step heating to synthesize CZTS nanocrystals, and all the reactions were conducted without inert gas protection. Though DDT could assist to passivate the obtained wurtzite CZTS through the strong coordination with the metal cations exposing on the surface of wurtzite CZTS NCs, wurtzite CZTS is still unstable and prone to transit from metastable wurtzite CZTS to stable kesterite CZTS. So, using pure DDT as the solvent (in the absence of OAm) always leads to the formation of two coexisting CZTS phases. As a strong ligand for Cu, Zn, and Sn,[10−12] OAm could cap the generated nanocrystals to reduce the surface energy and may prohibit the phase transition from metastable wurtzite CZTS to stable kesterite CZTS. So, it is rational to speculate that OAm adjusts the chemical environment preventing the phase transition from metastable wurtzite CZTS to stable kesterite CZTS. All these factors contribute to the formation of final metastable wurtzite phase CZTS and prevent the phase transition from metastable wurtzite to stable kesterite. In other words, OAm coordination to the metal cations exposing on the surface of wurtzite CZTS NCs has a kinetic effect on structure determination, or the presence of OAm has an influence on phase determination.

The morphology of the as-synthesized CZTS NCs synthesized with different amounts of OAm was investigated by TEM and shown in Figure 2. When pure DDT was used as the solvent, the as-synthesized CZTS NCs are mainly hexagonal nanoplates, and the obtained as-synthesized CZTS NCs is about 100−150 nm in diameter (Figure 2a). When a small amount of OAm (0.1−0.2 mL) was added to DDT, the hexagonal CZTS nanoplates became small, and some irregular polygon CZTS emerged (Figure 2b,c). When 0.5 mL of OAm was added to the reaction system, uniform and monodisperse rice-like CZTS NCs with an average size of about 50 nm were obtained (Figure 2d). If we continued to increase the concentration of OAm to 1.0 mL, the shape of the as-synthesized CZTS NCs are still rice-like, while the size distribution of the as-synthesized CZTS NCs become less uniform (Figure 2e). The corresponding HRTEM images of CZTS NCs obtained in pure DDT and with the participation of 0.5 mL of OAm are shown in Figure 2f,g. The HRTEM images of the as-synthesized CZTS NCs showed good crystallinity of the as-synthesized CZTS NCs (nanoplates and nanorices). The lattice fringe of CZTS nanoplates with an interplanar spacing of 0.32 nm was ascribed to the (002) plane of wurtzite CZTS; this result indicated the growth of wurtzite CZTS along the [002] direction. Actually, we had tried to find wurtzite−kesterite polytypism in CZTS nanoplates that we are aware of. However, we can not observe wurtzite−kesterite polytypism in CZTS nanoplates from TEM images due to experimental limitation. Apart from this, kesterite CZTS may constitute a relatively small portion of CZTS nanoplates, and the crystallinity of kesterite CZTS in CZTS nanoplates may be not very good. All these reasons may cause the failure of finding wurtzite−kesterite polytypism in CZTS nanoplates. For the CZTS nanorices, the interplanar spacing of the lattice fringe was 0.33 nm, which accounted for the growth of wurtzite CZTS along the (100) planes. The morphology of the as-synthesized CZTS NCs was also characterized by FESEM and shown in Figure S1 (Supporting Information). When pure DDT was used as the

dx.doi.org/10.1021/jp307346k | *J. Phys. Chem. C* 2012, 116, 26507−26516

solvent, most of the as-synthesized CZTS NCs are hexagonal nanoplates with average size of about 100−150 nm. When 0.5 mL of OAm was added to the reaction system, the as-synthesized CZTS NCs became small and uniform, the average size of the as-synthesized CZTS NCs is about 50 nm. These results correspond well with that of TEM characterizations.

In order to further study the element compositions of the as-synthesized CZTS NCs, the compositions of the as-synthesized CZTS NCs were confirmed using the energy dispersive spectroscopy, which are shown in Table S1 (Supporting Information). With the participation of different amounts of OAm, the morphology of the as-synthesized CZTS NCs changed greatly; however, the elemental composition of the as-synthesized CZTS NCs changed little. The elemental composition of the series of CZTS NCs synthesized with the participation of different amounts of OAm showed similar values of Cu/Zn/Sn/S ratio, which all basically agreed with the theoretical value of 2/1/1/4 (considering the error of the EDS detector). Elemental analysis spectra of two typical CZTS NCs samples (nanoplates, synthesized with pure DDT; nanorices, synthesized with DDT + 0.5 mL of OAm) are shown in Figure S2 (Supporting Information). The CZTS nanoplates showed an average value of Cu/Zn/Sn/S ratio of 1.99/1.26/1.15/4. The CZTS nanorices showed an average value of Cu/Zn/Sn/S ratio of 1.97/1.0/1.13/4, which is closer to the stoichiometry of CZTS.

Two typical CZTS NCs samples (nanoplates, synthesized with pure DDT; nanorices, synthesized with DDT + 0.5 mL of OAm) were further studied by Raman spectra, and the Raman scattering results over 200−500 cm^{-1} are shown in Figure 3.

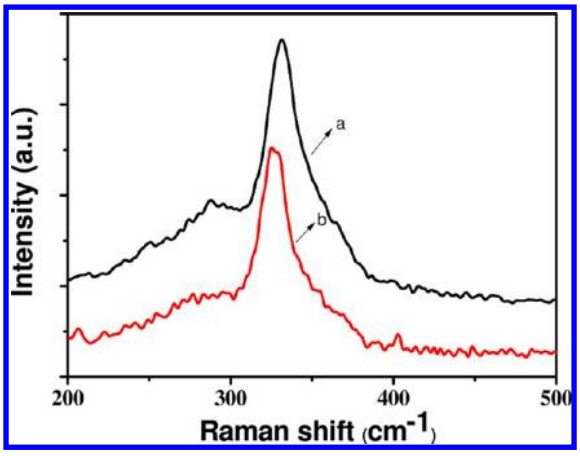

Figure 3. Raman spectrum of the (a) two coexisting phases and (b) pure metastable wurtzite CZTS NCs.

Though the Raman spectra of CZTS nanoplates and nanorices are quite similar, some differences were found. For CZTS nanoplates, an intense peak at 331 cm^{-1} and a weak peak at 288 cm^{-1} were observed (Figure 3a). For CZTS nanorices, a single Raman intense peak at 325 cm^{-1} was observed (Figure 3b). The reported Raman intense peak positions for kesterite CZTS are in the range from 331 to 338 cm^{-1}, while weak peak positions are in the range from 284 to 289 cm^{-1}.[3,14,21,22,28−33] The intense peak value for CZTS nanoplates is close to the minimum value, while the weak peak value is close to the maximum value. Meanwhile, the intense peak value for CZTS nanorices (pure phase wurtzite CZTS) is lower than the minimum of the reported values for kesterite CZTS. These phenomena indicated that the characteristic peak for wurtzite CZTS may differ from kesterite CZTS. The difference of characteristic intense peak may be caused by the different arrangements of atoms and belonging to different space groups. Except the above-mentioned Raman peaks, no other characteristic peaks of impurities were observed, such as $Cu_{2-x}S$ (475 cm^{-1}), ZnS (351 and 274 cm^{-1}), Cu_3SnS_4 (318, 348, and 295 cm^{-1}), SnS_2 (315 cm^{-1}), and so on.[2,3,14,21,22,28−33] These results excluded the presence of other binary or ternary compounds and confirmed the composition of as-synthesized CZTS nanorices by only wurtzite CZTS.

XPS analysis was used to study the valence states of all four elements in the as-synthesized wurtzite CZTS NCs (Figure 4). A survey spectrum of the as-synthesized wurtzite CZTS NCs identifies the presence of the Cu 2p, Zn 2p, Sn 3d, and S 2p (data not shown). The peak of Cu 2p is split into 931.6 ($2p_{3/2}$) and 951.4 eV ($2p_{1/2}$) with a split orbit of 19.8 eV, which is in good accordance with the value of Cu(I). The peaks of Zn 2p that appeared at binding energies of 1021.3 eV ($2p_{3/2}$) and 1044.6 eV ($2p_{1/2}$) with a peak splitting of 23.3 eV can be assigned to Zn(II). The peak of Sn 3d is split into 486.0 ($2p_{5/2}$) and 494.4 eV ($2p_{3/2}$) with a split orbit of 8.4 eV, which is in good accordance with the value of Sn(IV). The sulfur 2p peaks located at 161.4 ($2p_{3/2}$) and 162.6 eV ($2p_{1/2}$) with an energy difference of 1.2 eV is consistent with the 160 to 164 eV range of S in the sulphide phases. These results are consistent with the reported values in the literature.[20,22]

The UV−vis absorption spectra of CZTS nanoplates and nanorices are shown in Figure 5. The absorption spectra were measured using liquid phase method. The CZTS NCs were dispersed in tetrachloroethylene by ultrasound for several minutes, and then, the final solution was transferred to the cuvette to measure the absorption spectra. From Figure 5, we can see that all the CZTS NCs samples exhibited broad absorption in the visible region and that the tails extend to longer wavelengths. The band gaps were obtained by plotting $(Ah\nu)^2$ as a function of $h\nu$ (A = absorbance, h = Planck's constant, and ν = frequency). The corresponding band gaps of CZTS NCs are inserted in Figure 5. From the long wavelength extrapolation of the band edge, the values of the band gap for two kinds of NCs were determined to be 1.45 (nanoplates) and 1.49 eV (nanorices), respectively, which approach the optimum value for solar photoelectric conversion. The differences of absorption and band gaps may be caused by the morphology and size distribution of the CZTS NCs.

To study the electrical properties of the as-synthesized CZTS NCs, simple PV devices were fabricated with two typical CZTS NCs (nanorices and nanoplates). The fabrication details are as follows: the FTO glass was used as the substrate and was thoroughly washed with a mixed solution of deionized water, acetone, and 2-propanol (volume ratio of 1:1:1) under sonication for 60 min before fabrication of CZTS NCs films. CZTS NCs films were fabricated on FTO glass by the drop-coat method using a dense tetrachloroethylene solution of different CZTS NCs. After coating, the CZTS NC films were vacuum-dried at 60 °C, and then, a postanneal process was conducted in an Ar atmosphere at a rate of 2 °C/min and held at 500 °C for 30 min. At last, the PV devices were completed by RF sputtering of the Al electrode. As compared, kesterite CZTS films were also fabricated with pure kesterite CZTS NCs. Figure 6 shows the current−voltage curve of the different kinds of CZTS NC films measured in the dark (black) and under illumination (red). All the three kinds CZTS NC films

dx.doi.org/10.1021/jp307346k | J. Phys. Chem. C 2012, 116, 26507−26516

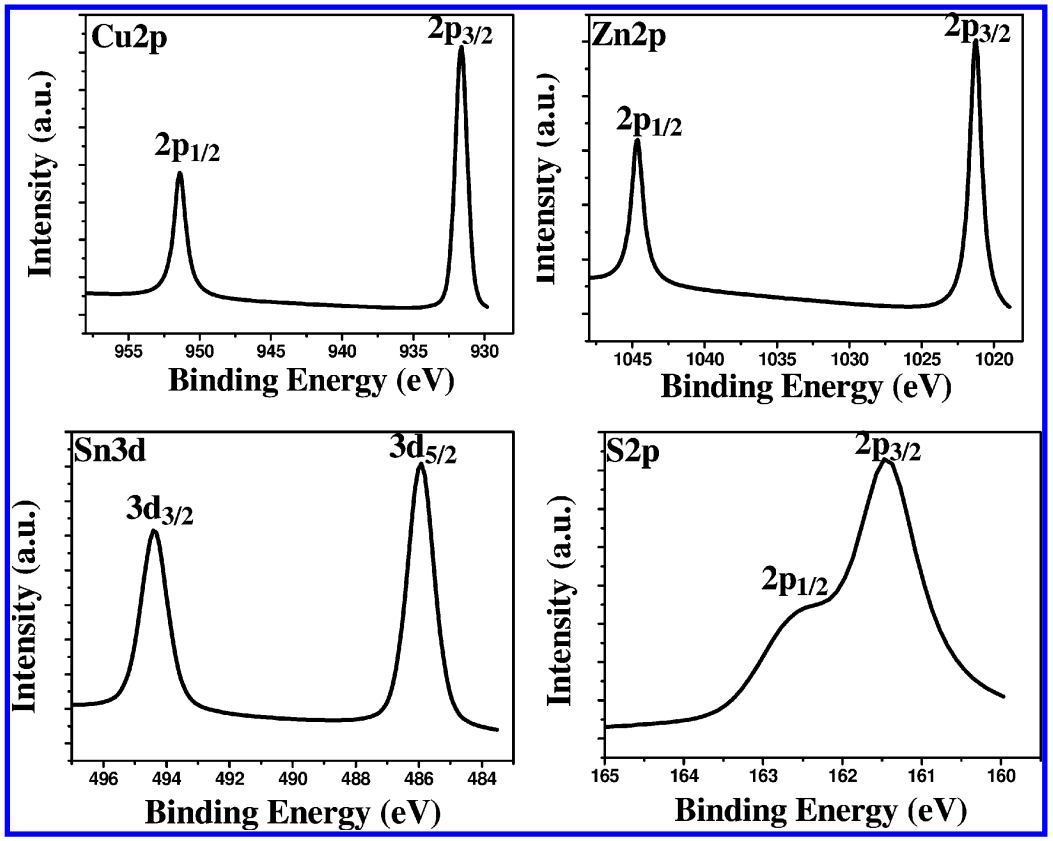

Figure 4. XPS of the pure metastable wurtzite CZTS NCs.

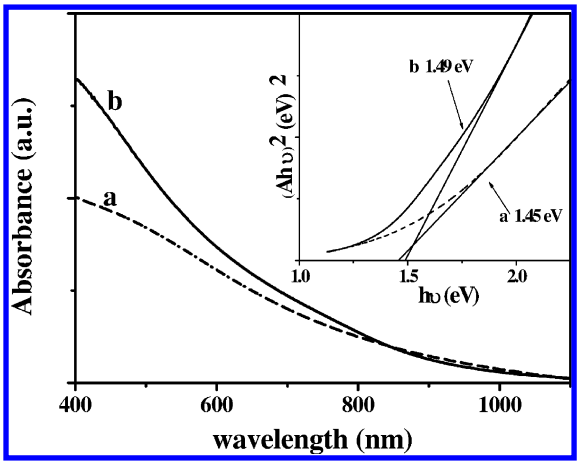

Figure 5. UV−vis absorption spectrum of (a) two coexisting phases CZTS NCs and (b) pure metastable wurtzite CZTS NCs. The optical band gap of the CZTS NCs was plotted at the right corner.

exhibited nearly linear current−voltage curves that are symmetric about the origin. The current increases linearly with the voltage, which implies the ohmic nature of the contacts. The lumination excites electrons in the valence band to the conduction band and then increases the holes in the CZTS, which enhance the conductivity of the as-obtained CZTS NCs films. Under illuminated conditions, at all bias voltages, the conductivity of the as-obtained CZTS NC films are higher compared to that under dark conditions. Compared to other CZTS (kesterite and coexisting CZTS) films, the wurtzite CZTS film showed higher conductivity rise under photon illumination. The photoconductivity of the CZTS NC films can be expressed by ΔI (the current difference in the dark and under illumination at a given bias voltage). At a bias voltage of −0.4 V, the coexisting CZTS and kesterite CZTS films exhibited weak photoconductivity of 0.26 mA and 0.20 mA, respectively. While, the wurtzite CZTS (nanorices) film exhibited relatively high photoconductivity of 0.81 mA. The photocurrent gain (characterized by I_{photon}/I_{dark}) in CZTS NCs films are 1.12, 1.13, and 1.32 for coexisting CZTS (nanoplates), kesterite CZTS, and wurtzite CZTS (nanorices), respectively. These results indicate that wurtzite CZTS nanorices are favorable to increase current carrier concentration and improve electron transmission.

In order to further study the electrical properties of kesterite CZTS and wurtzite CZTS, the carrier concentration, Hall mobility, and electrical resistivity were obtained by the four-probe method using Hall-effect measurement system in a magnetic field strength of 0.51 T at room temperature. The glass substrates were used to ensure that the conduction must come from the CZTS films rather than the substrates. Before electrical measurement, silver spot electrodes were made on CZTS films, and the ohmic contact between electrodes and CZTS films was confirmed. As shown in Table 1, the wurtzite CZTS films show a high carrier concentration of 1.47×10^{17} cm^3, low hall mobility of 4.31 cm^2/V s, and low resistivity of 8837.35 Ω cm, while the kesterite CZTS films show a low carrier concentration of 1.33×10^{15} cm^3, low hall mobility of 56.12 cm^2/V s, and high resistivity of 12443.36 Ω cm. These results provide further evidence that wurtzite CZTS are favorable to increase current carrier concentration and improve electron transmission.

3.2. Influence of the Reaction Conditions. As we all know, the reaction conditions (such as reaction temperature,

dx.doi.org/10.1021/jp307346k | J. Phys. Chem. C 2012, 116, 26507−26516

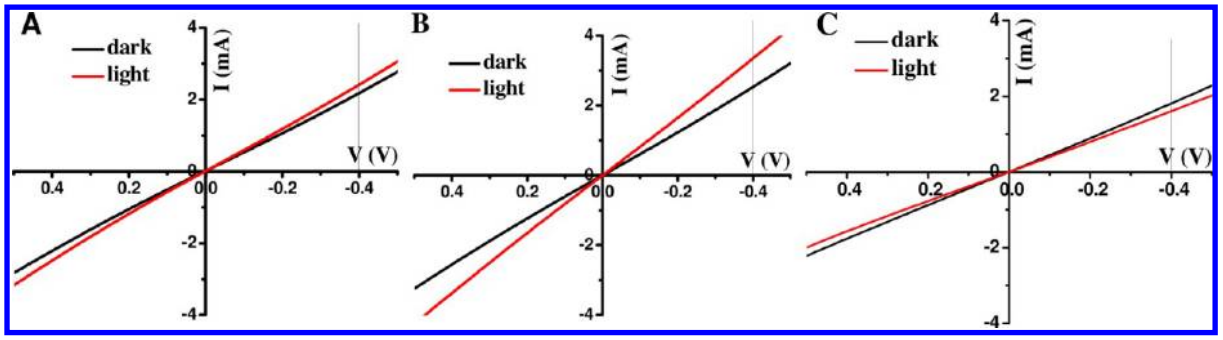

Figure 6. Current−voltage curve of the as-synthesized (A) two coexisting phase CZTS NCs, (B) pure metastable wurtzite CZTS NCs, and (C) pure kesterite CZTS NC films tested in the dark (black) and under light (red).

Table 1. Electrical Properties of Wurtzite CZTS NCs Film and Kesterite CZTS NCs Film Measured Using Hall-Effect Measurement System

sample	carrier concentration (cm^{-3})	Hall mobility ($cm^2/V\ s$)	resistivity (Ω cm)
wurtzite CZTS	1.47×10^{17}	4.31	8837.35
kesterite CZTS	1.33×10^{15}	56.12	12443.36

Table 2. Elemental Composition Values of CZTS NCs Synthesized by Changing the Reaction Factors According to the EDS Measurement

reaction condition	Cu/Zn/Sn/S	Cu/Zn + Sn
180 °C	2.65/1.26/0.70/4.00	1/0.74
200 °C	1.99/0.89/0.99/4.00	1/0.94
220 °C[a]	1.97/1.00/1.13/4.00	1/1.08
240 °C	1.97/1.34/1.20/4.00	1/1.29
0.5 C_0	2.29/1.34/1.14/4.00	1/1.08
2 C_0	2.40/1.01/0.94/4.00	1/0.81
5 C_0	3.29/1.05/0.77/4.00	1/0.55
0.5 h	7.76/1.78/0.77/4.00	1/0.33
1 h	3.37/1.00/0.79/4.00	1/0.53
2 h	2.95/1.35/1.20/4.00	1/0.86

[a]Typical experiment (C_0, 220 °C, 4 h).

reaction time, and concentration of precursors) have significant impacts on the morphology, size, and optical properties of the NCs. To ascertain the influence of the reaction conditions, shape evolution, and growth mechanism, we performed a number of experiments under different conditions, including adjusting of the reaction temperature (180 to 240 °C), the concentrations of the precursors (0.5 C_0 to 5 C_0; the concentration C_0 is the typical sample), and reaction time (0.5 to 24 h).

3.2.1. Influence of Reaction Temperature. During the growth process, the initial cream white solution gradually changed color to yellow, then changed to brown, and finally became black. When reaction temperature was set at 220 °C, the initial solution changed color to brown-black within around 10 min, and the color change occurred within 20 min for a relatively low reaction temperature (180 or 200 °C) and 5 min for high reaction temperature (240 °C), respectively. The XRD patterns of the CZTS NCs prepared at different temperatures (180 to 240 °C) for 4 h are shown in Figure S3 (Supporting Information). It can be seen that all the major diffraction peaks of the samples can be indexed to the phase of wurtzite CZTS. The intensity of diffraction peaks increase gradually with the increase of the reaction temperature, indicating the improvement of the crystallinity. It should be noted that tiny extra impurity peak appearing at about 38° was observed in the reaction products when the reaction temperature was lower than 220 °C. Composition analysis by EDS showed the values of the average composition and Cu/(Zn + Sn) ratio of the CZTS NCs obtained at different reaction temperatures (Table 2 and Table S2 (Supporting Information)). When synthesized at 220 °C, the average Cu/Zn/Sn/S composition and Cu/(Zn + Sn) ratio of CZTS NCs were 1.97/1.0/1.13/4.00 and 1/1.08, respectively. These values are quite close to the stoichiometry of CZTS. When synthesized at 180 °C, a much higher Cu/(Zn + Sn) ratio of 1/0.74 was obtained. When the reaction temperature was set at 200 °C, a more stoichiometric composition of CZTS was obtained (1.99/0.89/0.99/4.00), and the Cu/(Zn + Sn) ratio reduced to 1/0.94 (still copper-rich), while when the reaction temperature was set at 240 °C, the Cu/(Zn + Sn) ratio was too low (1/1.29). Therefore, a best temperature of 220 °C was required to obtain the typical CZTS NCs.

3.2.2. Influence of Reaction Concentration. The influence of precursor concentration in the range from 0.5 C_0 to 5 C_0 was studied. The XRD patterns of the as-synthesized CZTS NCs at different concentrations are shown in Figure S4 (Supporting Information). When the precursor concentration varied from 0.5 C_0 to 2 C_0, the XRD peaks of the as-obtained CZTS NCs matched well with the wurtzite CZTS. The precursor concentration has little influence on crystallinity of the as-obtained CZTS NCs. When precursor concentration increased to 5 C_0, XRD peak broadening was observed, and some impurity peaks also appeared. The influence of reaction concentration on CZTS NC elemental composition was also studied. CZTS NCs were synthesized at 220 °C, and the reaction concentration varied from 0.5 C_0 to 5 C_0. Composition analysis by EDS showed the values of the average composition, and Cu/(Zn + Sn) ratios of the CZTS NCs are shown in Table 2 and Table S3 (Supporting Information). When the concentration was C_0, the average Cu/Zn/Sn/S composition and Cu/(Zn + Sn) ratio of CZTS NCs were 1.97/1.0/1.13/4.00 and 1/1.08, respectively. When synthesized at relatively low concentration (0.5 C_0), the average Cu/Zn/Sn/S composition and Cu/(Zn + Sn) ratio of CZTS NCs were 2.29/1.34/1.14/4.00 and 1/1.08, respectively. These values are quite close to the stoichiometry of CZTS. When the concentration increased to 2 C_0 and 5 C_0, the ratio of the Cu/(Zn + Sn) become 1/0.81 and 1/0.55, respectively. These

dx.doi.org/10.1021/jp307346k | J. Phys. Chem. C 2012, 116, 26507−26516

results demonstrated that low concentration was required to obtain ideal CZTS NCs.

3.2.3. Influences of Reaction Time. The XRD patterns of the nanocrystals isolated from the reaction mixture at different time (from 30 min to 24 h) are shown in the Figure 7. Before

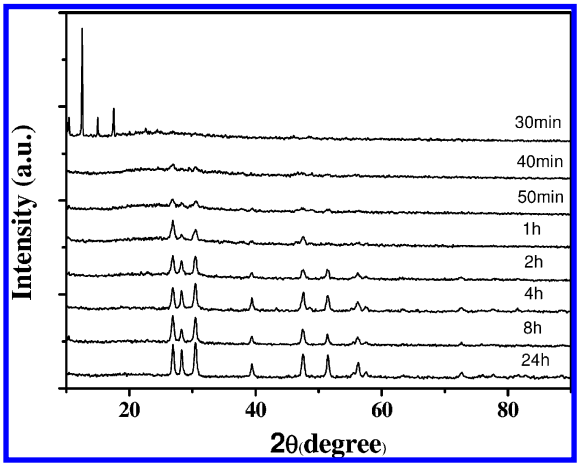

Figure 7. XRD patterns of CZTS products synthesized at different reaction times.

30 min, CZTS NCs were not formed, and organic precursor still existed in the product. As the reaction time prolonged, the intensity of the diffraction peaks increased gradually, which indicated the gradual formation of the CZTS NCs. In order to ascertain the growth and shape evolution of CZTS nanorices, detailed time-dependent evolution of morphology was studied by TEM and shown in Figure 8. When the reaction proceeded for 30 min, the dominant products are sphere-like (or disc-like) NCs with average size of about 10 nm (Figure 8a). As the reaction time was prolonged, rhombus-like NCs were observed (Figure 8b–d). When the reaction proceeded for 1 h, the dominant products are rhombus-like NCs with diameter of 25–30 nm, and several rice-like NCs are also present (Figure 8d). When the reaction time was increased to 2 h, most of the rhombus-like NCs changed to rice-like NCs (nanorices) with diameter of about 30 nm (Figure 8e). As the reaction time was prolonged to 4 h, only nanorices with diameter of about 40 nm were observed. When the reaction time was continually increased to 8 or 24 h, the shape of the NC was unchanged, and the diameter increased quite little. Therefore, 4 h was required to obtain CZTS nanorices. The UV–vis absorption spectra of CZTS NCs obtained in different times are shown in Figure 9A. The absorption spectra were measured using liquid phase method. The CZTS NCs were dispersed in tetrachloroethylene by ultrasound for several minutes, and then, the final solution was transferred to the cuvette to measure the absorption spectra. The UV–vis absorption spectra of the CZTS NCs synthesized at different time exhibit broad absorption in the visible region. As the time prolonged, the absorption edge of NCs gradually shifts toward longer wavelengths. From the long wavelength extrapolation of the band edges, the band gap values for all of the obtained NCs were determined to be 2.01, 1.74, 1.59, and 1.49 eV corresponding to 30 min, 1 h, 2 h, and 4 h, respectively. The relationship between the diameter and band gap of the CZTS NCs was also studied. The evolutions of the band gap and size of the NCs with different reaction times (30 min to 4 h) are shown in the Figure 9B. As the reaction time prolonged, the size of CZTS NCs gradually increased from ~10 to ~40 nm, while the band gap value of the NCs gradually decreased from 2.01 to 1.49 eV (narrowing of the optical energy band gap upon increasing their crystal size due to the quantum size effect). The compositions, Cu/Zn + Sn ratios, and Zn/Sn ratios of CZTS NCs obtained at different reaction times are shown in Tables 2 and 3. As the reaction time prolonged, the Cu/Zn + Sn ratio reduced from 1/0.33 to 1/1.08, while the Zn/Sn ratio reduced from 1/0.43 to 1/1.13, and a best stoichiometric composition (1.97/1.0/1.13/4.00) of CZTS was obtained when the reaction time prolonged to 4 h, which is quite close to the theoretical value of 2:1:1:4.

3.3. Growth and Formation Mechanism. On the basis of the above detailed time-dependent shape evolutions (Figure 8) and elemental composition evolutions (Table 3), a possible

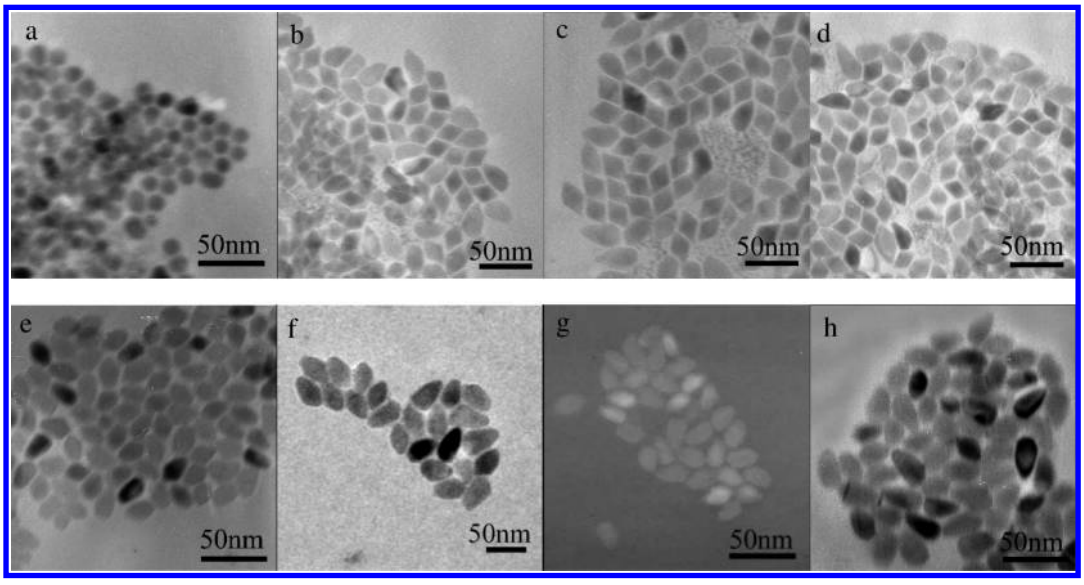

Figure 8. TEM images of the CZTS products synthesized at different reaction times: (a) 30 min, (b) 40 min, (c) 50 min, (d) 1 h, (e) 2 h, (f) 4 h, (g) 8 h, and (h) 24 h, respectively.

dx.doi.org/10.1021/jp307346k | J. Phys. Chem. C 2012, 116, 26507–26516

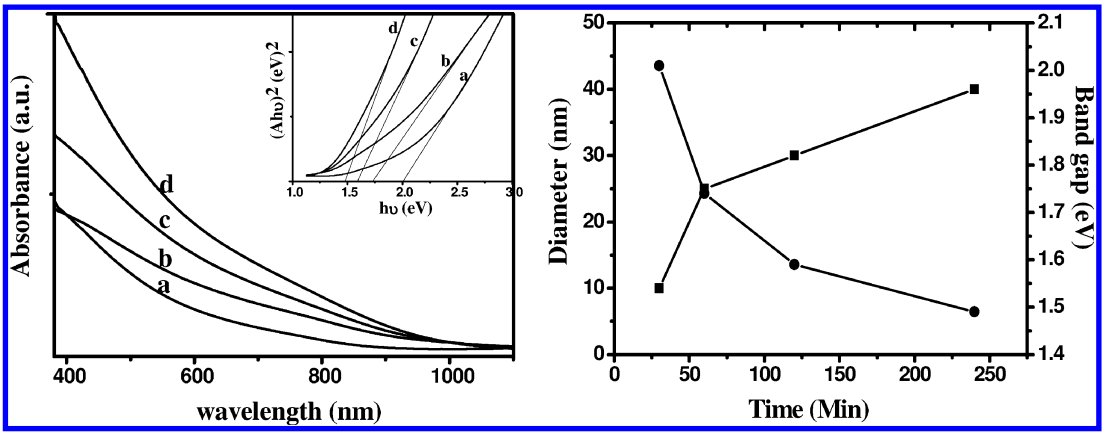

Figure 9. (left) UV−vis absorption spectrum of CZTS NCs synthesized for different reaction times; (a) 30 min, (b) 1 h, (c) 2 h, and (d) 4 h. The optical band gap of CZTS NCs was plotted in the inset of panel a. (right) Evolutions of the diameter and band gap of the NCs with different reaction times: ■, diameter of the NCs; ●, band gap of the NCs.

Table 3. Elemental Composition Values of CZTS Products Synthesized by Changing the Reaction Times According to the EDS Measurement

area	0.5 h	1 h	2 h	4 h
Cu/Zn/Sn/S (area 1)	54.11/13.97/4.30/27.62	37.40/11.41/9.40/41.79	27.25/12.93/12.11/47.72	22.82/11.48/14.38/51.32
Cu/Zn/Sn/S (area 2)	54.39/11.08/6.92/27.61	35.69/12.04/7.97/44.30	32.52/12.71/13.44/41.34	22.65/12.26/13.92/51.17
Cu/Zn/Sn/S (area 3)	54.16/12.23/5.0/28.61	37.23/9.24/8.53/45.00	33.44/16.98/12.45/37.13	27.56/13.32/13.59/45.61
Cu/Zn/Sn/S (average)	54.22/12.43/5.41/27.95	36.77/10.90/8.63/43.70	31.07/14.21/12.67/42.06	24.34/12.35/13.96/49.37
Cu/Zn/Sn/S	7.76/1.78/0.77/4.00	3.37/1.0/0.79/4.00	2.95/1.35/1.20/4.00	1.97/1.0/1.13/4.00
Cu/Zn + Sn	1/0.33	1/0.53	1/0.86	1/1.08
Zn/Sn	1/0.43	1/0.79	1/0.89	1/1.13

formation mechanism was proposed and illustrated in Figure 10. Here, we call it the asynchronous doping growth

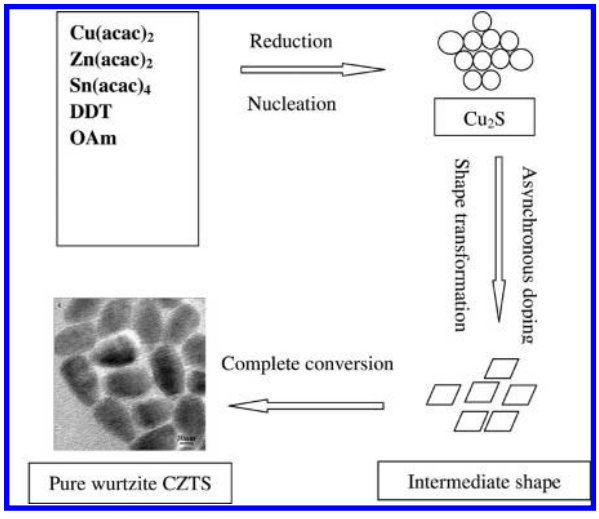

Figure 10. Schematic illustrations of the formation process for rice-like wurtzite CZTS NCs.

mechanism. The formation process of final CZTS nanorice NCs may be divided into three steps. First, the rapid formation (nucleation) of Cu_2S occurred with the help of OAm. Second, the asynchronous doping of Zn and Sn assisted growth and shape transformation to rhombus-like intermediate shaped NCs. Finally, conversion was complete, and pure wurtzite CZTS NCs were obtained. During the typical growth process, the color of the solution gradually changed from initial cream white to yellow, then changed to brown and finally became black, which is related to the CZTS NC formation and growth. With the magnetic stirring, metal ions (Lewis acid) complexed with DDT (Lewis base) in solution to form metal−DDT thiolates, which would decompose into corresponding sulfides at certain temperature.[19,23−25] These thiolates help to balance the different reactivities of cations in solution. During the first 30 min, because of the reduction of DDT and activation of OAm, the Cu−DDT complexes were first thermally decomposed to form spherical-like Cu_2S. The spherical-like morphology (Figure 8a) was also consistent with the shape of Cu_2S in many other reports.[21,26,27] UV−vis absorption spectra of the first samples taken out of the reaction mixture show the typical absorption of an indirect semiconductor and can be assigned to copper sulfide [Figure 9a, left]. A high copper content [Cu/(Zn + Sn) = 1:0.33)] in the samples also taken in the beginning 30 min reveals the first formation of Cu_2S (Table 3). The first of formation of Cu_2S can be explained by the smallest solubility-product constant of 2.5×10^{-48}. Because of the similar anionic framework (anion lattices) of Cu_2S and CZTS, the interdiffusion of cations between the two materials becomes possible as there is little lattice distortion.[21] At relatively high reaction temperature, the copper ions in Cu_2S have a relatively high mobility, which can facilitate an exchange with other metal ions.[26] So, the typical reaction condition (220 °C) believed to facilitate the chemical transformation from Cu_2S to CZTS. As the time proceeds, Zn^{2+} and Sn^{4+} were gradually incorporated into the crystal lattice of formed Cu_2S and replaced parts of Cu^+, which was confirmed from Cu/(Zn + Sn) ratio evolutions (Table 2). At the same time, the shape of the sample transformed from spherical-like to rhombus-like intermediate shape. Owing to the ionic radius of Zn^{2+} (74 pm) being closer to that of Cu^+ (77

dx.doi.org/10.1021/jp307346k | J. Phys. Chem. C 2012, 116, 26507−26516

pm) than Sn^{4+} (69 pm), Zn^{2+} will be preferentially doped into Cu_2S over Sn^{4+}, resulting in an asynchronous doping. With the reaction time prolonged, zinc content in the samples gradually reached the theoretical value, which induced the relatively high doping speed of tin. When the reaction time was prolonged to 4 h, the Zn/Sn ratio reduced to 1/1.13, which matched with the theoretical value of 1:1. Finally, rice-like wurtzite CZTS NCs were formed from the rhombus-like intermediate shaped NCs. In order to further clarify the role of OAm at the initial stage, time-dependent experiments without the use of OAm were also performed. The XRD patterns and the elemental composition values of the as-synthesized CZTS nanoplate NCs at different reaction times are showed in Figure S5 and Table S4, respectively (Supporting Information). As an organic base, OAm can serve as an activating agent, which could expedite the precursor decomposition process of metal compounds.[34] In the absence of OAm, the product showed an average value of Cu/S ratio of 1.76/1 at the early stage (0.5 h). This value is lower than that of the product prepared with the use of OAm (1.94/1). This result indicated that the early stage products maybe quite different when OAm is used or not. In other words, the early stage product prepared without the use of OAm may not be Cu_2S. XRD patterns of the early stage products prepared without the use of OAm are also quite different from the early stage products in the presence of OAm. On the basis of the above mentioned, we can draw the conclusion that OAm indeed helps the formation of Cu_2S at the nucleation step. Thus, the OAm not only serves as a stabilizer to maintain the wurtzite phase at the growth stage but also serves as an activating agent inducing the formation of Cu_2S at the nucleation step.

4. CONCLUSIONS

In summary, the pure phase rice-like wurtzite CZTS NCs have been successfully synthesized by a facile one-pot route. The key factor deciding the formation of wurtzite CZTS rather than kesterite CZTS is the DDT used in the reaction, while pure DDT used as the solvent introduced two coexisting CZTS phases (wurtzite CZTS is unstable and prone to transit stable kesterite CZTS). When some amount of OAm was added to DDT, OAm adjusted the chemical environment and prevented the phase transition from metastable wurtzite CZTS to stable kesterite CZTS. Time-dependent experiments revealed the final CZTS NCs evolved from spherical-like Cu_2S NCs through rhombus-like intermediate shape NCs to rice-like pure wurtzite CZTS NCs. On the basis of the detailed time-dependent shape and elemental composition evolutions, a possible asynchronous doping growth and formation mechanism was proposed. The UV−vis absorption spectra revealed that the pure wurtzite CZTS NCs had an absorption in the visible wavelength range, indicating its potential application as a solar absorber. Meanwhile, the $I-V$ curve showed that the pure wurtzite CZTS NCs favored the generation of photoinduced carrier and electronic transmission. The synthesis strategy developed in this work may be used as a general process for the synthesis of pure wurtzite CZTS NCs and may have great potential to be applied in high efficiency, yet low cost photovoltaic areas.

■ ASSOCIATED CONTENT

Ⓢ Supporting Information

FESEM images, elemental analysis spectrum, XRD patterns, Raman spectrum, elemental composition values. This material is available free of charge via the Internet at http://pubs.acs.org.

■ AUTHOR INFORMATION

Corresponding Author

*Tel: +86-378-3881358. Fax: +86-378-3881358. E-mail: zhouwh@henu.edu.cn (W.-H.Z.); wusixin@henu.edu.cn (S.-X.W.).

Notes

The authors declare no competing financial interest.

■ ACKNOWLEDGMENTS

This project is supported by the National Natural Science Foundation of China (20871041, 20903033, 21203053, and 21271064), the Joint Talent Cultivation Funds of NSFC-HN (U1204214), the New Century Excellent Talents in University (NCET-08-0659), the Program for Changjiang Scholars and Innovative Research Team in University (PCS IRT1126), the Scientific Research Foundation of Henan University (SBGJ090510 and 2010YBZR014), and the Doctoral Scientific Research Foundation of Henan University (B2010079).

■ REFERENCES

(1) Katagiri, H. *Thin Solid Films* **2005**, *480481*, 426−432.
(2) Katagiri, H.; Jimbo, K.; Yamada, S.; Kamimura, T.; Maw, W. S.; Fukano, T.; Ito, T.; Motohiro, T. *Appl. Phys. Express* **2008**, *1*, 041201.
(3) Zhou, Y. L.; Zhou, W. H.; Li, M.; Du, Y. F.; Wu, S. X. *J. Phys. Chem. C* **2011**, *115*, 19632−19639.
(4) Wang, H. X.; Bell, J. *Int. J. Photoenergy* **2011**, 801292.
(5) Nakayama, N.; Ito, K. *Appl. Surf. Sci.* **1996**, *92*, 171−175.
(6) Katagiri, H.; Nishimura, M.; Onozawa, T.; Maruyama, S.; Fujita, M.; Sega, T.; Watanabe, T. *Proc. Power Convers. Conf.* **1997**, *2*, 1003−1006.
(7) Shin, B.; Gunawan, O.; Zhu, Y.; Bojarczuk, N. A.; Chey, S. J.; Guha, S. *Prog. Photovoltaics* **2011**, DOI: 10.1002/pip.1174.
(8) Barkhouse, D. A. R.; Gunawan, O.; Gokmen, T.; Todorov, T. K.; Mitzi, D. B. *Prog. Photovoltaics* **2012**, *20*, 6−11.
(9) Bag, S.; Gunawan, O.; Gokmen, T.; Zhu, Y.; Todorov, T. K.; Mitzi, D. B. *Energy Environ. Sci.* **2012**, *5*, 7060−7065.
(10) Guo, Q. J.; Hillhouse, H. W.; Agrawal, R. *J. Am. Chem. Soc.* **2009**, *131*, 11672−11673.
(11) Riha, S. C.; Parkinson, B. A.; Prieto, A. L. *J. Am. Chem. Soc.* **2009**, *131*, 12054−12055.
(12) Steinhagen, C.; Panthani, M. G.; Khavan, V. A.; Goodfellow, B.; Koo, B.; Korgel, B. A. *J. Am. Chem. Soc.* **2009**, *131*, 12554−12555.
(13) Guo, Q. J.; Ford, G. M.; Yang, W. C.; Walker, B. C.; Stach, E. A.; Hillhouse, H. W.; Agrawal, R. *J. Am. Chem. Soc.* **2010**, *132*, 17384−17386.
(14) Zou, C.; Zhang, L. J.; Lin, D. S.; Yang, Y.; Li, Q.; Xu, X. J.; Chen, X. A.; Huang, S. M. *CrystEngComm* **2011**, *13*, 3310−3313.
(15) Kameyama, T.; Osaki, T.; Okazaki, K.; Shibayama, T.; Kudo, A.; Kuwabata, S.; Torimoto, T. *J. Mater. Chem.* **2010**, *20*, 5319−5324.
(16) Persson, C. *J. Appl. Phys.* **2010**, *107*, 053710.
(17) Shavel, A.; Arbiol, J.; Cabot, A. *J. Am. Chem. Soc.* **2010**, *132*, 4514−4515.
(18) Fischereder, A.; Rath, T.; Haas, W.; Amenitsch, H.; Albering, J.; Meischler, D.; Larissegger, S.; Edler, M.; Saf, R.; Hofer, F.; Trimmel, G. *Chem. Mater.* **2010**, *22*, 3399−3406.
(19) Lu, X. T.; Zhuang, Z. B.; Peng, Q.; Li, Y. D. *Chem. Commun.* **2011**, *47*, 3141−3143.
(20) Singh, A.; Geaney, H.; Laffir, F.; Ryan, K. M. *J. Am. Chem. Soc.* **2012**, *134*, 2910−2913.
(21) Regulacio, M. D.; Ye, C.; Lim, S. H.; Bosman, M.; Ye, E. Y.; Chen, S. Y.; Xu, Q. H.; Han, M. Y. *Chem.—Eur. J.* **2012**, *18*, 3127−3131.
(22) Jiang, H. C.; Dai, P. C.; Feng, Z. Y.; Fan, W. L.; Zhan, J. H. *J. Mater. Chem.* **2012**, *22*, 7502−7506.
(23) Xie, R. G.; Rutherford, M.; Peng, X. G. *J. Am. Chem. Soc.* **2009**, *131*, 5691−5697.

(24) Zhuang, Z. B.; Peng, Q.; Zhang, B.; Li, Y. D. *J. Am. Chem. Soc.* **2008**, *130*, 10482−10484.
(25) Choi, S. H.; An, K.; Kim, E. G.; Yu, J. H.; Kim, J. H.; Hyeon, T. *Adv. Funct. Mater.* **2009**, *19*, 1645−1649.
(26) Kruszynska, M.; Borchert, H.; Parisi, J.; Kolny-Olesiak, J. *J. Am. Chem. Soc.* **2010**, *132*, 15976−15986.
(27) Li, X. M.; Shen, H. B.; Niu, J. Z.; Li, S.; Zhang, Y. G.; Wang, H. Z.; Li, L. S. *J. Am. Chem. Soc.* **2010**, *132*, 12778−12779.
(28) Li, Z. Q.; Shi, J. H.; Liu, Q. Q.; Chen, Y. W.; Sun, Z.; Yang, Z.; Huang, S. M. *Nanotechnology* **2011**, *22*, 265615.
(29) Altosaar, M.; Raudoja, J.; Timmo, K.; Danilson, M.; Grossberg, M.; Krustork, J.; Mellikov, E. *Phys. Status Solidi A* **2008**, *205*, 167−170.
(30) Grossberg, M.; Krustok, J.; Raudoja, J.; Timmo, K.; Altosaar, M.; Raadik, T. *Thin Solid Films* **2011**, *519*, 7403−7406.
(31) Mitzi, D. B.; Gunawan, O.; Todorov, T. K.; Wang, K.; Guha, S. *Sol. Energy Mater. Sol. Cells* **2011**, *95*, 1421−1436.
(32) Shi, L.; Pei, C. J.; Xu, Y. M.; Li, Q. J. *J. Am. Chem. Soc.* **2011**, *133*, 10328−10331.
(33) Ahmed, S.; Reuter, K. B.; Gunawan, O.; Guo, L.; Romankiw, L. T.; Deligianni, H. *Adv. Energy Mater.* **2012**, *2*, 253−259.
(34) Pan, D. C.; Wang, X. L.; Zhou, Z. H.; Chen, W.; Xu, C. L.; Lu, Y. F. *Chem. Mater.* **2009**, *21*, 2489−2493.